Desalination and Water Treatment
www.deswater.com
doi: 10.5004/dwt.2022.28991

277 (2022) 177–189
November

Adsorption of levofloxacin antibiotic residuals from wastewater onto mesoporous ZnO nanoparticle: equilibrium, kinetics, and thermodynamics

Khuloud A. Alibrahim

Department of Chemistry, College of Science, Princess Nourah bint Abdulrahman University, P.O. Box 84428, Riyadh 11671, Saudi Arabia, email: kaalibrahim@pnu.edu.sa/dr.kbrahim@yahoo.com

Received 3 June 2022; Accepted 4 October 2022

ABSTRACT

This research demonstrates the preparation, characterization and the regarding of levofloxacin (LEV) that is removed from actual wastewater samples using zinc oxide as an absorbent. ZnO nanosphere appeared with 41.6 nm as average particle-size and with 94.19 $m^2.g^{-1}$ as a Brunauer–Emmett–Teller surface area. Adsorption equilibrium models for the LEV's adsorption behavior on ZnO nanospheres, kinetics, and thermodynamics were investigated. Kinetics models demonstrated that both intraparticle and outside diffusion regulated the adsorption mechanism. Furthermore, the obtained outcomes revealed that the adsorption of LEV onto ZnO was dominated by chemisorption processes including electrostatic contact, complex formation, fluoride substitution, and hydrogen bonding. Moreover, Dubinin–Radushkevich and Temkin isotherms showed that chemisorption was the dominant sorption process. Monolayer adsorption was supported by the Langmuir model. The highest LEV adsorption effectiveness onto ZnO adsorbent was set at 570.25 $mg{\cdot}g^{-1}$. Additionally, Information on the thermodynamics of the adsorption process showed that it was spontaneous and endothermic and was supported by the Temkin isotherm model. The synthesized ZnO nanosphere shows important reusability and up to five adsorption–desorption cycle renewability features. The produced adsorbent's effectiveness was assessed for laboratory scale purifying of spiked real water samples as a proof-of-concept. The amount of LEV was greatly lowered by the produced adsorbent. In actual water samples, the removal rate ranged from 85.17% to 97.28%.

Keywords: Levofloxacin antibiotic; ZnO nanosphere; Adsorption kinetics; Adsorption isotherms

1. Introduction

Antibiotics are frequently used in animals and humans [1]. Antibiotics have been discovered in soils, and sediments. There is groundwater and surface water as a result of their discharge into the environment all over the world. Their concentrations in surface waters vary from zero to tens of thousands of milligrams per liter [2–4]. Antibiotics can affect the composition of microbial communities in natural settings leading to antimicrobial resistance in some microorganisms [5–7].

Water contamination in both surface and underground sources has harmed the ecology and health and has limited the amount of fresh water that may be consumed [8]. The most frequent and dangerous contaminants found in industrial wastewaters rank high on this list. Over the past 10 y, reports from several researchers have indicated that Pharmaceuticals businesses now produce 200,000 tons of antibiotics annually that are increased approximately 100,000 tons previously. The fact that these antibiotics are vital substances used to treat a variety of bacterial infections affecting both humans and animals. This fact is still focusing in many researches. Antibiotics can eventually be identified in water systems when they are misused or handled incorrectly. These will have severe effects on human

health when they penetrate food crops and drinking water supplies. They will also increase the number of bacteria that are resistant to antibiotics, which is now recognized as a global environmental issue [9]. Additionally, antibiotics have negative effects on agricultural products when they contaminate the soil and water. This can limit respiration, affect microbial growth, interfere with nitrification, and prevent iron absorption among other effects on plant growth (III). Therefore, it is vital to manage and reduce the adverse effects of antibiotics that are present in the environment especially in wastewater and is high in antibiotics [10,11].

Because a wide range of pharmaceutical medications including such antibiotics are frequently consumed, huge amounts of antibiotics are mostly discharged into the surroundings from pharmaceutical makers after human used it for the treatment of a variety of maladies by humans and animals [12,13]. A large fraction of the given dose is released as an active component into aquatic effluents [14]. As a result, several types of pharmaceutical chemicals are in surface water and wastewater, so they have been subjected to water treatment for years through many interrelated investigations [15]. Regardless of the reality that these chemicals found in low doses makes them difficult to investigate, their persistence in drinking water for an extended length of time may have considerable negative impacts on human and environmental health [16]. Although these materials are present in low amounts, it is hard to evaluate them and their presence in drinking water for an extended length of time may have considerable negative impacts on the environment and human health [17]. Treating wastewater technologies including activated sludge are insufficient for the total removal of active pharmaceutical chemicals and other wastewater elements [18]. As a result, the current approaches can only isolate 60%–90% of antibiotics [19]. For its basic design, simplicity use, and relatively simple renewal, it is a popular choice, the adsorption approach has been used to clean the environment of a wide range of antibiotic contaminants [20–22].

Fluoroquinolone synthetic compounds are commonly antibiotics that have been used to treat common illnesses for both animals and humans [23]. Levofloxacin (LEV) is a fluoroquinolone antibiotic (FQs) and it is a relatively new antibiotic with a broad spectrum of activities that are synthesized. Many types of squandered biomass, activated carbon has lately been produced from date palm leaflets, lotus stem, peat, and the husks of trepanations and FQs antibiotics can be extracted from water solution with this device [23–25].

LEV is a fluoroquinolone antibiotic with a variety of options has been used by both human and veterinary medicines with extensive use [26]. Furthermore, LEV is beneficial in the treatment of infections in the lower and upper respiratory tracts, as well as the epidermis, genitourinary, gynecological, and soft tissues [27–29]. LEV has also been shown to be useful for the treatment of cutaneous [30,31]. Furthermore, LEV has broad antibacterial properties and potentially affected diseases including both harmful and beneficial microorganisms. Furthermore, LEV has a low rate of biodegradation making it challenging to extract it from wastewater by utilizing conventional biological techniques [32,33]. As a result, developing effective strategies for completely removing LEV from environmental matrices is critical. The research aims to make ZnO nanospheres for adsorptive LEV from an aqueous solution and investigates the effect of pH, contact time, LEV concentration, adsorption temperature, kinetics, isotherm, and thermodynamic investigations. With the help of these substances, the adsorption technique between LEV and ZnO nanosphere was studied.

2. Materials and methods

2.1. Materials and instruments

The materials and instruments used for characterization were illustrated in detail in (Supplementary information).

2.2. Preparation of the ZnO nanoparticles

The ZnO was attained by the calcination of $[ZnLCl(OH_2)]H_2O$ chelate (Fig. 1) at the temperatures of 450°C, 550°C, and 650°C for 4 h [33] This method produces ZnO nanoparticles easily without the use of expensive and harmful solvents or complicated equipment.

2.3. Preparation of adsorbate

LEV's standard solution (2.5×10^{-3} mol·L^{-1}) was put in a volumetric flask and was dissolved in water, then it has been distilled twice by using double-distilled water, and finally the stock solution was diluted to the proper concentration to create the workable solutions [34].

2.4. Adsorption experiments

To avoid the degradation due to light exposure, all adsorption studies were conducted in a flask with a flat bottom and an aluminum foil seal while being vigorously stirred. In a nutshell, suitable quantities (0.02–0.25 mg) were inserted into a 25 mL round bottom flask of the adsorbent and it should be added a 100 mL model solution containing 10 mg·L^{-1} of LEV (pH ranging between 2 and 12). After that, the adsorption is measured by using a UV Spectrophotometer at wavelength 298 nm. Finally, the solutions were positioned on a water bath shaking at a varying speed of 2–4 at a fixed temperature (298 K) and at a different temperature to investigate the effect of temperature on Lev adsorption optimization of dosage, temperature, time, and pH [35].

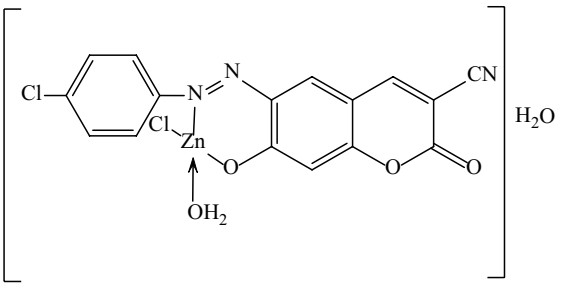

Fig. 1. Proposed structures of $[ZnLCl(OH_2)]H_2O$.

Calculations of LEV's adsorption capacity and % elimination were made using Eqs. (1) and (2), respectively (Supplementary information):

$$q_e = \frac{(C_0 - C_e)V}{m} \quad (1)$$

$$\%R = \frac{(C_0 - C_t)}{C_0} \times 100 \quad (2)$$

3. Results and discussion

3.1. Characterization of ZnO

3.1.1. X-ray diffraction patterns

Fig. 2 depicts the X-ray diffraction (XRD) pattern of ZnO at various temperatures. The creation of the tetragonal structure with lattice constants can be seen in the measured diffraction peaks associated with well crystallised NiO $a = b = 16.16$ Å, $c = 2.56$ Å, $\alpha = 90.0°$, $\beta = 90°$ and $\gamma = 120°$. That indicates the existence of ZnO in triagonal. The interplanar spacing (d_{hkl}) and Miller indices (*hkl*) for ZnO are recorded in Table 1 (JCPDS Card No. 01-089-0510). Also, formation energy/atom was –1.776 eV, energy above hull/atom 0.023 eV and band gap 0.738 eV. No extra peaks were detected due to contamination. This is considered great evidence of the high purity of produced ZnO's. Also, the XRD patterns of ZnO samples at various temperatures are similar. The crystal planes (100), (002), (001), (102), (110), (103), (112), and (201) of bulk ZnO can be easily indexed at 2θ = 32.24°, 34.89°, 63.37°, 48.65°, 75.31°, 63.4°, 68.5°, and 69.66°, respectively. By using the Scherrer formula [34] the ZnO nanoparticles' crystallite size (*D*) was estimated (Fig. 2).

3.1.1.1. Crystallite size and strain determination

3.1.1.1.1. Scherrer method

A polycrystalline configuration of the ZnO at 450°C, 550°C, and 650°C nanoparticles was suggested since the peak positions and strength ratios. The size of crystallite ZnO nanoparticles was determined using the Scherrer formulation. Eq. (3) was used to predict the diffraction's peak of ZnO adjusted experimental broadening, β_{hkl} (Supplementary information).

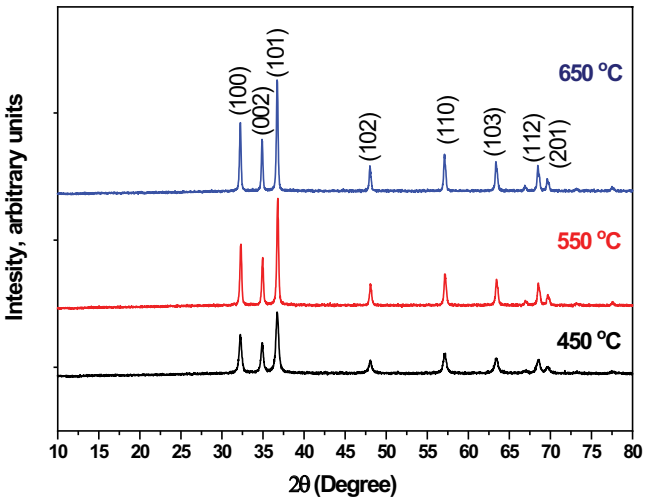

Fig. 2. XRD of ZnO at different calcination temperatures (450°C, 550°C and 650°C).

$$\beta_{hkl} = \left[(\beta_{hkl})^2_{measured} - \beta^2_{instrumental} \right]^{1/2} \quad (3)$$

It is widely known that the Scherrer formula [Eq. (4)] only gives the crystallite size's lowest bound. By using the Scherrer formula, the size of crystalline nanoparticles is determined (Table 2).

$$d = \frac{K\lambda}{\beta \cos\theta} \quad (4)$$

3.1.1.1.2. Williamson–Hall method

3.1.1.1.2.1. Uniform deformation model

In several instances, there are factors that affect crystallite size; lattice strain and lattice defects on the X-ray diffraction peaks. The Williamson–Hall study is a condensed version of the integral breath approach and distinguishes between the peak of distortion caused by the strain and the armature size and the widening of the peak as a function of 2θ. Individual contributions to a Bragg reflection of line broadening can be written as follows in Eq. (5):

$$\beta_{hkl} = \beta_S + \beta_D \quad (5)$$

It is expected that the strain is constant along the crystallographic direction in the Williamson–Hall relationship, which is given by β_{hkl} – Eqs. (6)–(9):

Table 1
Crystallography of ZnO

$2\theta_{Obs.}$ (°)	$2\theta_{Calc.}$ (°)	$d_{hkl(Obs)}$ (Å)	$d_{hkl(Calc.)}$ (Å)	*hkl*
32.248	32.262	2.7758	2.7747	350
34.899	34.932	2.5708	2.5684	001
36.739	36.711	2.4462	2.448	021
48.065	48.046	1.8929	1.8936	380
57.14	57.122	1.612	1.6124	561
63.415	63.417	1.4667	1.4667	191
68.538	68.546	1.3691	1.3689	1001
69.663	69.66	1.3497	1.3498	1021

Table 2
Geometric parameter of ZnO nanoparticles

Methods	Parameter	Calcination temperature (°C)		
		450	550	650
Scherrer	*D* (nm)	22.12	29.32	33.35
Williamson–Hall	*D* (nm)	22.48	30.105	33.89
UDM	ε	0.25	0.075	0.11

$$\beta_{hkl} = \frac{K\lambda}{D\cos\theta} + 4\varepsilon\tan\theta \quad (6)$$

$$\beta_{hkl}\cos\theta = \frac{K\lambda}{D} + 4\varepsilon\tan\theta \quad (7)$$

$$D = \frac{K\lambda}{Y\ \text{Intercept}} \quad (8)$$

$$\varepsilon = \text{Slope} \quad (9)$$

The average grain size has increased [34]. The rising extent of the accumulation of ZnO particles can be used to explain these findings. By calculating the particle-size using two methods Scherrer and Williamson–Hall uniform deformation model (UDM), the result were similar and close to each other.

3.1.2. Brunauer–Emmett–Teller surface area

Fig. 3 illustrates the pore size of Barrett–Joyner–Halenda (BJH) distribution curves of ZnO and the isotherms of nitrogen adsorption at 77 K. The N_2 adsorption–desorption isotherms are typically typed II with a distinct "knee" that at low pressures, while at high pressures, it appears to be nearly parallel to the pressure axis according to the IUPAC classification and hysteresis loops implying a mostly microporous nature among the relative pressure. According to P/P_0, and the adsorption–desorption graphs, there are well-defined stages. The existence of a restricted dispersion of mesopores is suggested by a value of 0.4–1.0. A desorption hysteresis loop served as a sign of this (H_3/H_4 type) coupled with slit-shaped holes, micropores are being demonstrated (<2 nm) and mesopores (2–50 nm) at the same time. The Brunauer–Emmett–Teller (BET) surface area of ZnO is quite large 94.19 $m^2 \cdot g^{-1}$ and an average pore size of 2.79 nm so the pores could be classified as mesoporous. BJH has a pore size of 1.4477 nm on average, which is suitable for adsorption [36].

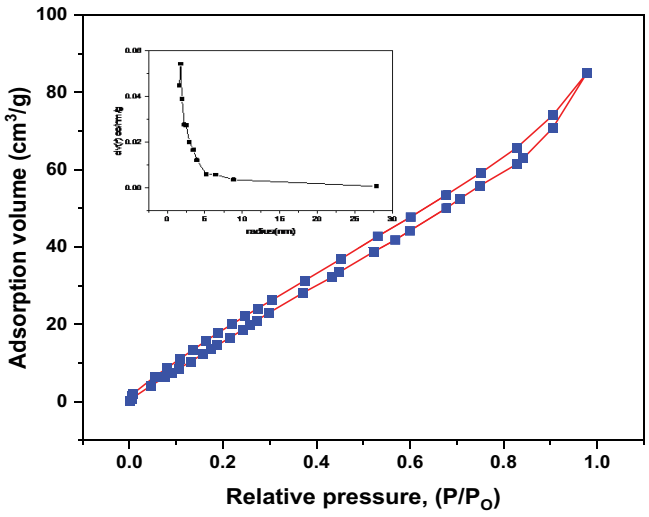

Fig. 3. For the ZnO nanosphere, isotherms of N_2 adsorption–desorption.

3.1.3. Scanning electron microscopy analysis

To evaluate the morphological and structural characteristics of ZnO, scanning electron microscopy (SEM) examination was performed. Fig. 4 shows the SEM study ZnO at 450°C nanoparticles with an average diameter of 41.6 nm were discovered. As the calcination temperature increased, the ZnO grew longer [34,37].

3.1.4. Determination of point of zero charge (pH_{PZC})

Results of pH_{PZC} value for ZnO at 450°C was shown in Fig. 5. The pH_{PZC} value of 5 for the ZnO at 450°C was determined. This result indicated that whenever the pH of the solution is less than 5, the ZnO surface possesses a positive charge that makes anionic adsorbate adsorption easier, while the pH of the solution is more than 5, the surface charge is negative [34,37,38].

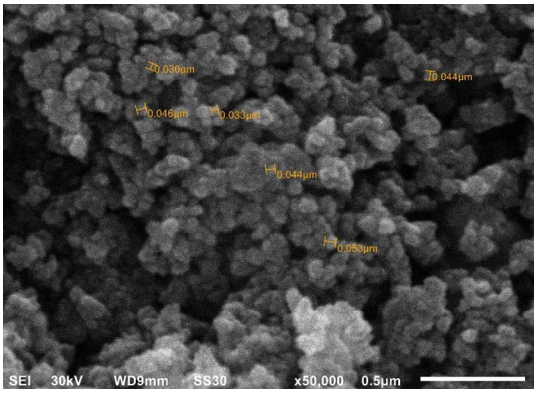

Fig. 4. SEM picture of ZnO at calcination temperature of 450°C.

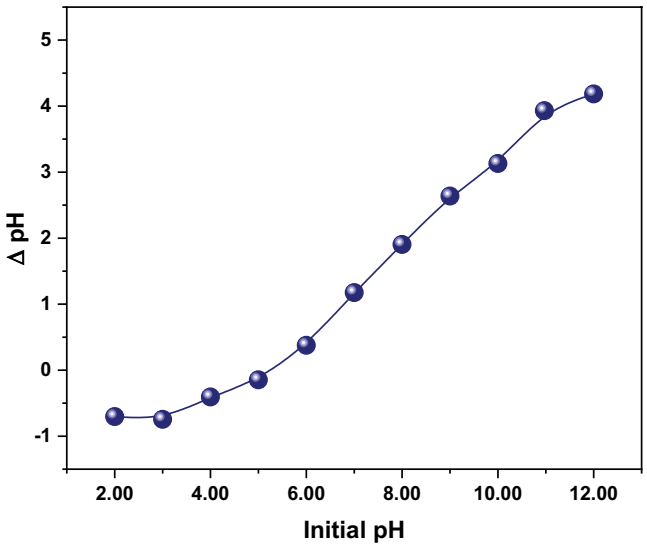

Fig. 5. Starting pH and the ΔpH of ZnO are related at the calcination temperature of 450°C.

3.2. Batch experiments

3.2.1. Effect of pH

Fig. 6 shows how pH affects the structure and adsorption of LEV. The LEV Cationic compounds are the most common (protonated piperazinyl group, H_2L^+) under pH 5, anionic (deprotonated carboxyl group, L^-) over pH 8.5, and zwitterionic (or neutral, HL^0) at pH between its pK_{a1} and pK_{a2} values. The desorption of the LEV molecules at various pH levels and its substance sorption is significantly affected. Fig. 7 depicts the adsorption of LEV onto ZnO at various pH levels. At a pH of roughly 6, LEV's adsorbed concentration reaches a peak. Once the pH is lower or higher, it lowers. There is a pH-dependent in an earlier study on the adsorption of other antibiotics with a similar structure [39]. The quantity of adsorbed ciprofloxacin on goethite is equal to the highest concentration of LEV adsorbed. At pH < 5, both the ZnO surface and the LEV in the solution have a positive charge. Chemical adsorption, in particular, will be blamed for the adsorption. On both LEV and ZnO, the positive charge increases, pH values decreases. The protonated amine groups on LEV molecules are increasingly repelling one another. As the pH fell, less LEV was absorbed and the positively ZnO surface charged ($pH < pH_{PZC}$). Antibiotics with a piperazinyl group were less likely to bind to ZnO nanospheres, particularly when the pH is low. The highest adsorption of LEV was seen at pH 6, which is near to LEV's pK_{a1}.This signifies that a major portion of the population (about 50%) is under this pH and the carboxylic group on LEV is deprotonated. For the sorption of several organic acids to ZnO nanospheres, comparable adsorption behavior has also been reported, where maximum adsorption occurs at pH values near to the pH values of protonation in functional groups. At varied pH levels (3–12), the adsorption of LEV by ZnO was investigated at starting concentrations of 1.9×10^{-3} mol·L^{-1} of the LEV, 25°C, and 0.02 g adsorbent dosage.

3.2.2. Effect of calcination temperature

The Impact of ZnO calcination temperature on LEV adsorption process was tested using ZnO at various

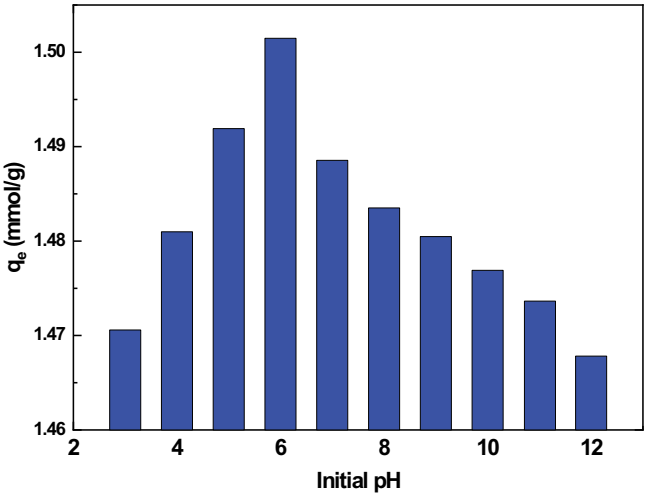

Fig. 7. pH effect on LEV adsorption using ZnO (*T*: 25°C; C_0: 1.9×10^{-3} mol·L^{-1}).

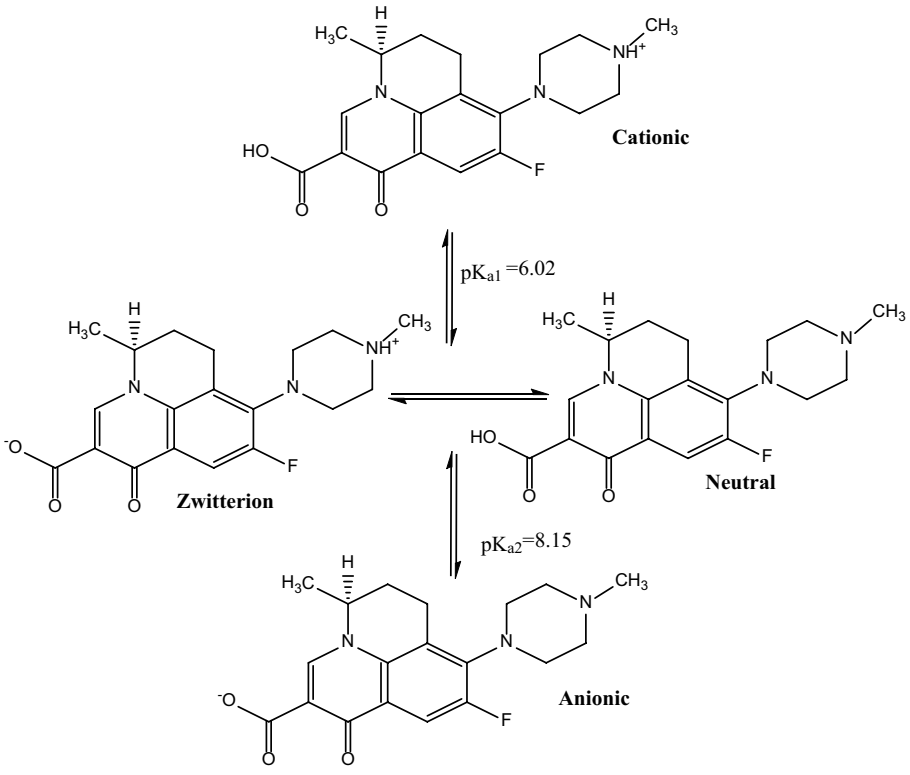

Fig. 6. pH-dependent speciation and molecular structure.

calcination temperatures at 450°C, 550°C, and 650°C. ZnO dose was 0.02 g; the LEV solution volume was 25 mL; and the concentration was 1.22 × 10^{-3} mol·L^{-1}, while shaking frequency was 200 rpm, and the pH was 6. The adsorption efficiency of LEV fell from 99.8% > 83.79% > 82.23% by using ZnO at 450°C, 550°C, and 650°C, respectively as increasing the particle-size as the temperature of calcination increased. This means the higher adsorption for the LEV will occur on the adsorbent ZnO's tiny particles at 450°C. The enhanced availability of binding sites was associated with a greater surface area for bulk LEV adsorption (Fig. 8) [40,41].

3.2.3. Effect of dose

The impact of different ZnO amounts and pH 6 0.02–0.25 g per 25 mL on the LEV concentration of 1.9x10^{-3} mol·L^{-1} at 25°C is shown in Fig. 9. As the dose of ZnO was increased from 0.01 to 0.25 g, the q_e was decreased from 1.49 to 0.13 mmol·g^{-1}, respectively. This increase from a larger surface area allows the vacant site to reach specified limit in a fixed number of LEV molecules. When the dose increased, the adsorbent's surface area increased, but the equilibrium concentration of (LEV) decreases [42].

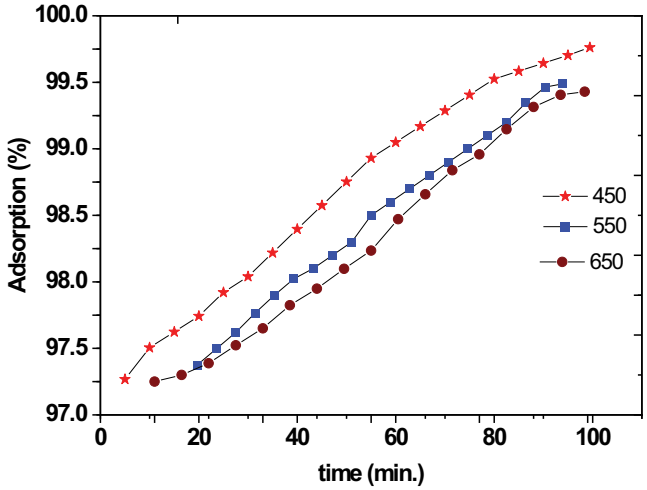

Fig. 8. Effect of particle-size of ZnO nanoparticles on the adsorption of LEV.

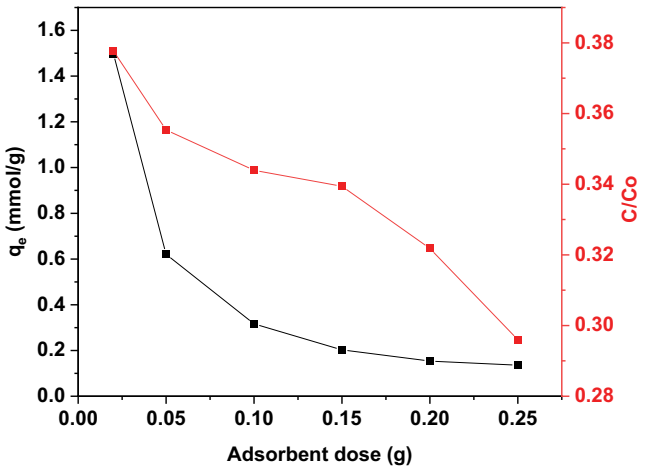

Fig. 9. Effect of ZnO dosage on the adsorption of LEV.

3.2.4. Effect of initial concentration

Influence concentration of examined dyes LEV on ZnO at 450°C was studied at LEV concentrations ranging from 8.85 × 10^{-4} to 3.6 × 10^{-3} mol·L^{-1} and 0.02 g dosage of ZnO at 450°C. According to LEV at pH 6 over time, it reaches a maximum value of 100 min (Fig. 10). When LEV concentration increased the removal decreased. The effective receptors of ZnO at 450°C deteriorated with increasing LEV concentrations resulted in a percentage drop in adsorption [43].

3.2.5. Adsorption isotherm

The reaction of LEV with ZnO nanosphere was studied using adsorption isotherms [Eqs. (10)–(13)]. It shows the quantity of adsorbate per mass of ZnO, and it is used to evaluate adsorption operations. LEV adsorbs to ZnO nanospheres at equilibrium shown in Fig. 11 and it can be observed in this graph. The adsorbed amount of LEV increases dramatically with increasing the equilibrium concentration (C_e) and the maximum adsorption capacity was 571.012 mg·g^{-1} [44].

$$\text{Langmuir: } \frac{C_e}{q_e} = \frac{1}{q_m K_L} + \frac{C_e}{q_m} \tag{10}$$

$$\text{Freundlich: } \ln q_e = \ln K_F + \frac{1}{n}\ln C_e \tag{11}$$

$$\text{Dubinin–Radushkevich: } \ln q_e = \ln Q_{DR} - K_{DR}\varepsilon^2 \tag{12}$$

$$\text{Temkin: } q_e = \beta_T \ln K_T + \beta_T \ln C_e \tag{13}$$

Isotherm models in four different forms (Langmuir, Freundlich, Dubinin–Radushkevich, and Temkin) were

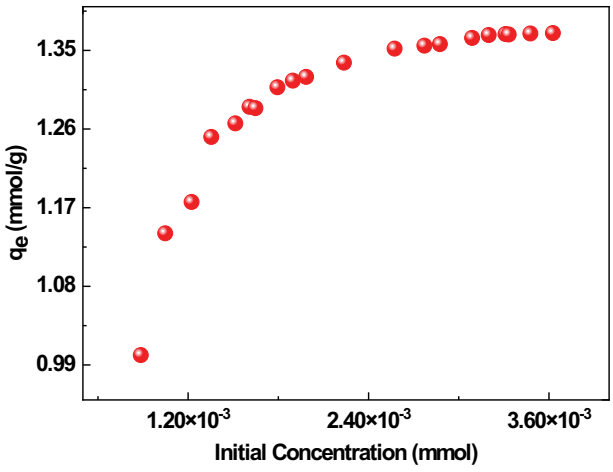

Fig. 10. Effect of initial concentration of LEV.

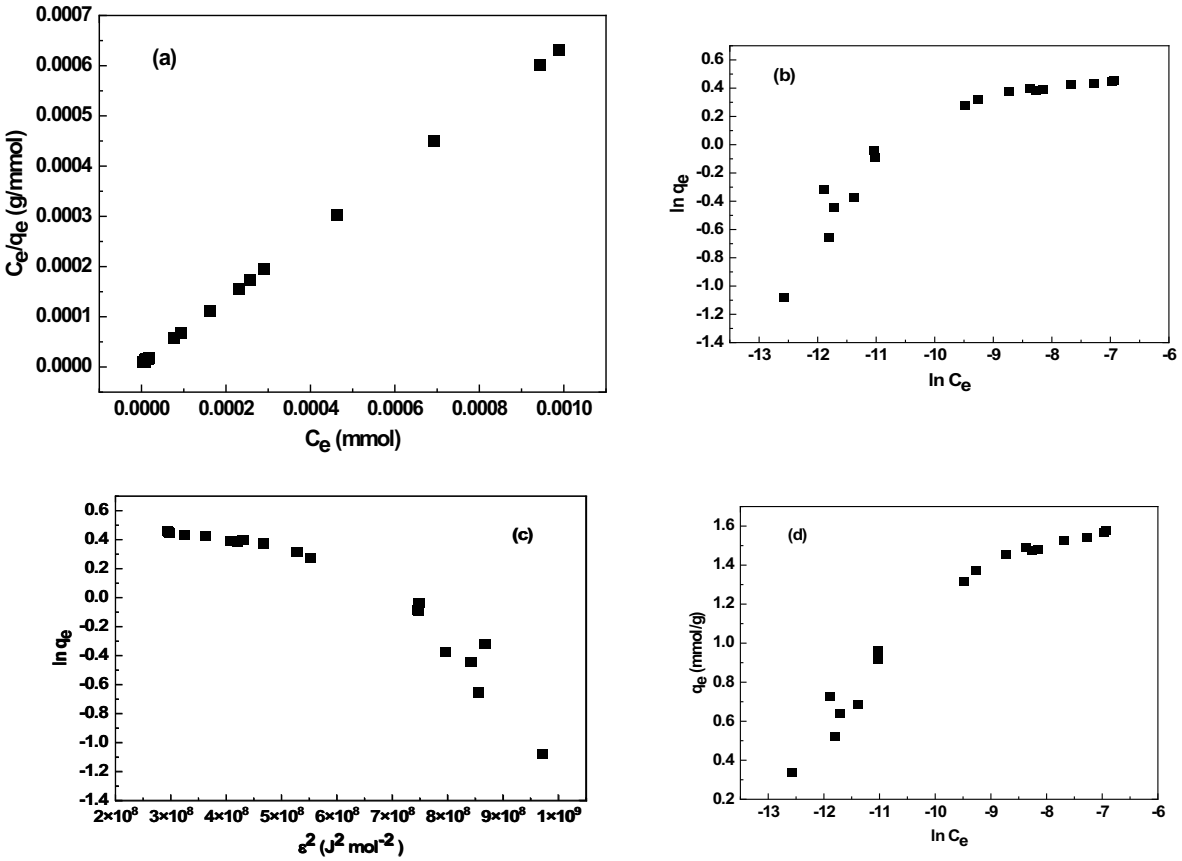

Fig. 11. LEV sorption isotherm linearized plots: (a) Langmuir equation, (b) Freundlich equation (c) Dubinin–Radushkevich, and (d) Temkin.

Table 3
Fitting parameters for the isotherm models of LEV adsorbed on ZnO nanosphere

Isotherm	Value of parameters	
Langmuir	$q_{m,exp}$ (mmol·g^{-1})	1.5779
	q_m (mmol·g^{-1})	1.5814
	K_L (L·mmol^{-1})	72,186.073
	R^2	0.9999
Freundlich	n	4.48732
	K_F (mmol·g^{-1})(L·mmol^{-1})$^{1/n}$	1.244
	R^2	0.713
Dubinin–Radushkevich	q_{DR}	1.17199
	K_{DR} (J^2·mol^{-2})	–1.919E-09
	E_a (kJ·mol^{-1})	16.14
	R^2	0.8738
Temkin	b_T (L·mol^{-1})	11,605.096
	A_T (kJ·mol^{-1})	14.96
	R^2	0.92487

studied and Table 3 presented the parameters computed using linear plots (Fig. 11). As it is connected to the Freundlich model, the adsorption of LEV revealed high correlation coefficient value for the Langmuir. The obtained results showed that LEV is adsorbed on a monolayer surface indicating chemisorption. The physical and chemical adsorption of LEV (E) onto ZnO nanospheres were differentiated using the Dubinin–Radushkevich isotherm under the assumption of Gaussian energy distribution. If the measured value of E falls below a predetermined cut-off point, adsorption can be classified as physical. If it is below (8 kJ·mol^{-1}) or classified as chemical, it is higher than (8 kJ·mol^{-1}) depending on the value. Additionally, it can be verified that the adsorption was defined by chemisorption based on the computed E value (Table 3).

It was possible to test the adsorption using the Langmuir isotherm model. The Temkin isotherm was used to study how indirectly adsorbate/adsorbent relationships affected the adsorption process. Moreover, it's rational to assume that the adsorption heat is significant (ΔH_{ads}). The layer's total particle decreases linearly with increasing the covered surface area. The Temkin isotherm is used to demonstrate that LEV adsorptions on ZnO nanospheres are chemisorption processes. Moreover, depending on the outcomes b_T value as established in Table 3, the endothermic nature of the adsorption indicates that it was driven by electrostatic interaction between the LEV and the adsorbent. Finally, by evaluating their correlation cofficiencies, the level to which these models fit (R^2) follows the sequence: Langmuir > Temkin > Dubinin–Radushkevich > Freundlich.

3.2.6. Adsorption kinetics

According to the rate and the process of adsorption for LEV onto ZnO nanosphere, the kinetic data was adjusted to pseudo-first-order [45] and pseudo-second-order as shown in Fig. 12. The linear equations [Eqs. (14)–(17)] were employed to investigate these models, as well as the resulting pseudo-first-order and pseudo-second-order. Table 4 displays kinetic models, all LEV concentrations were evaluated, and the resulting data revealed that the pseudo-second-order model is suitable. Their large regression coefficient value confirms this ($R^2 > 0.999$) that is applicable with pseudo-first-order model, so the chemisorption process is suggested. Moreover, the pseudo-second-order order kinetic model's predicted the adsorption rate (q_e) values were closer to those found in the experiment values. According to these observations, the chemisorption process, which involves covalent forces, accounted for the largest share LEV adsorption between the surface functional groups of the adsorbent and the LEV zwitterion form. Furthermore, an intraparticle diffusion model was used to examine the rate limitation in the adsorption mechanism. Previous research has found that if adsorbed a plot of LEV is plotted, the rate-determining step is intraparticle diffusion (Table 4 and Fig. 12). In either, it was shown that the plot did not go through the origin but it showed multi-linearity suggesting intraparticle diffusion that was not the sole factor affecting rate. Rapid external surface adsorption is represented by the first steeper linear segment and intraparticle diffusion is the rate-regulating phase in

Table 4
Parameters for the kinetic models of LEV adsorbed on ZnO nanosphere

Model	Value of parameters	
Pseudo-first-order kinetic	K_1 (min^{-1})	–0.0144
	q_e ($mmol{\cdot}g^{-1}$)	0.12885
	R^2	0.88588
Pseudo-second-order kinetic	K_2 ($g{\cdot}mg^{-1}{\cdot}min^{-1}$)	0.477799
	q_e ($mmol{\cdot}g^{-1}$)	1.5747
	R^2	0.99975
Intraparticle diffusion	K_i ($mg{\cdot}g^{-1}{\cdot}min^{-1/2}$)	0.00517
	X ($mg{\cdot}g^{-1}$)	0.06414
	R^2	0.92685
Elovich	β ($g{\cdot}mg^{-1}$)	–168.067
	α ($mg{\cdot}g^{-1}{\cdot}min^{-1}$)	1.0507
	R^2	0.25347
Experimental data	$q_{e,exp}$ ($mmol{\cdot}g^{-1}$)	1.5779

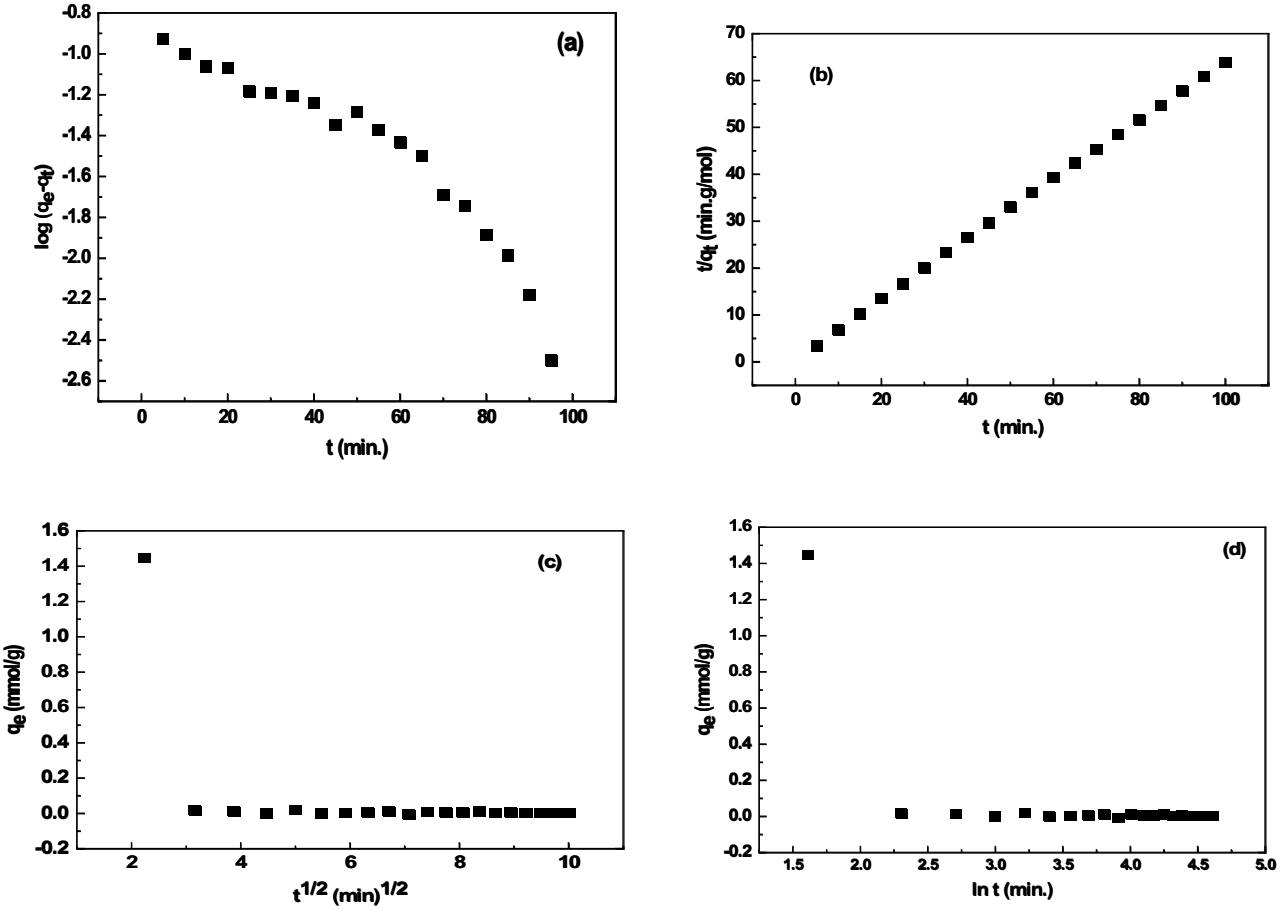

Fig. 12. Modeling of uptake kinetics for LEV with (a) pseudo-first-order rate expression, (b) pseudo-second-order rate expression, (c) simplified model of resistance to intraparticle diffusion (Morris and Weber equation), and (d) Elovich equation.

the continuous adsorption of LEV, but the second section serves as a representation. The intraparticle diffusion rate constant is shown in Table 4, k_{id}, for the adsorption of LEV onto ZnO nanosphere. The intercept, X decreased, while the adsorption of LEV onto ZnO nanosphere increased.

Pseudo-first-order model: $$\log\left(q_e - q_t\right) = \log q_e - \left(\frac{K_1}{2.303}\right)t \quad (14)$$

Pseudo-second-order: $$\frac{t}{q_t} = \frac{1}{K_2 q_e^2} + \frac{t}{q_e} \quad (15)$$

Intraparticle diffusion: $$q_t = K_i t^{1/2} + X \quad (16)$$

Elovich: $$q_t = \frac{1}{\beta}\ln\left(\alpha\beta\right) + \frac{1}{\beta}\ln t \quad (17)$$

3.2.7. Thermodynamics

The adsorption isotherm of LEV onto ZnO nanosphere at numerous temperatures (293, 298, 303, 308, and 318 K) were demonstrated in Table 5. $\Delta G°$ was calculated using Eqs. (18) and (19) in describing the LEV onto ZnO nanosphere thermodynamic performance. Based on the obtained results of ΔG (–9.26, –10.96, –12.56, –14.35, –16 and –17.73 kJ·mol^{-1}), the adsorption occurred spontaneously. The fact that the ΔH values have a negative sign and it shows that the adsorption mechanism was endothermic. The ΔS and ΔH values were found to be 338.46 J·mol^{-1}·K^{-1} and kJ·mol^{-1} respectively demonstrating that chemisorption is favored by the adsorption system [46,47].

$$\ln K_C = -\frac{\Delta H°}{RT} + \frac{\Delta S°}{R} \quad (18)$$

$$\Delta G° = \Delta H° - T\Delta S° \quad (19)$$

3.2.8. Effect of ionic strength (addition of NaCl)

To test the performance of ZnO at 450°C, ionic strength's effectiveness towards LEV was comprehensively simulated. The quantity of additional rival (co-interfering) ions in the aqueous solution has a considerable impact on LEV purification as shown in Fig. 13. There is a slight decrease in ZnO at 450°C loading capacity, while the competitor's density has increased (i.e., Cl^-). The ZnO adsorption capacities are still impressive of 1.39 mmol·g^{-1} for LEV. The struggle between charged anionic ions is intensifying (Cl^-) negatively and LEV molecules interact with the ZnO at 450°C adsorbent surface. Furthermore, increasing the concentration of electrolyte counter ions leads to protecting the ZnO at 450°C surface and slowing the adsorption process (Fig. 13). Furthermore, as the solution salinity increased, the double electric layer was compressed resulting in a repulsive force between the LEV and the adsorbent surface. Other studies have found that inorganic competitors have antagonistic effects on LEV adsorption using diverse adsorbents, which is a more honest description [47].

3.3. Adsorption mechanism

Fig. 14 displays the ZnO nanosphere's Fourier-transform infrared (FT-IR) spectra before and after the adsorption of

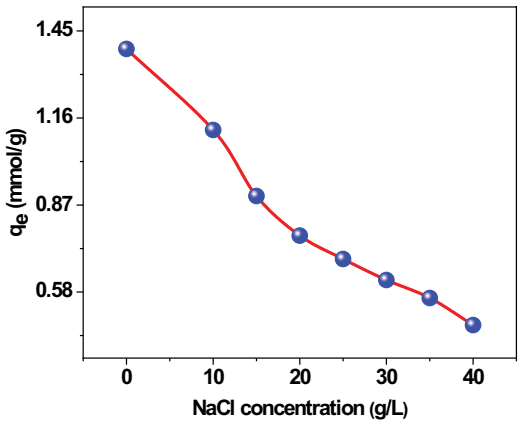

Fig. 13. NaCl affects the adsorption of LEV onto ZnO at 450°C.

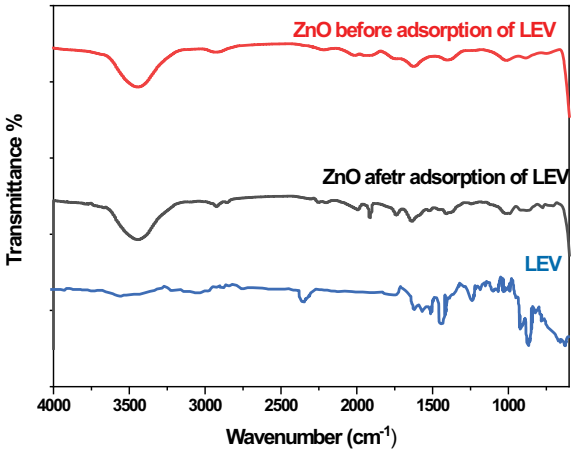

Fig. 14. FT-IR spectra of LEV and ZnO before and after adsorption of LEV.

Table 5
Standard $\Delta G°$, $\Delta S°$, and $\Delta H°$ for LEV on ZnO

Adsorbate	$\Delta H°$ (kJ·mol^{-1})	$\Delta S°$ (J·mol^{-1}·K^{-1})	T_0 (K)	$\Delta G°$ (kJ·mol^{-1})					
				293 K	298 K	303 K	308 K	318 K	318 K
LEV	89.899	338.46	265.61	–9.26	–10.96	–12.56	–14.35	–16.0	–17.73

LEV. At 3,451 cm^{-1}, the ZnO nanosphere displayed a large peak, and this was explained by the stretching of the O–H. A bridging bidentate complex was created when the Zn from the adsorbent joined the O atom of the carboxyl group, which caused the O–H stretching vibrations for the carboxylic group at 3,272 cm^{-1} to vanish LEV. When the LEV molecule is adsorbing, the carboxylic group peaks at about 1,719 cm^{-1} vanished demonstrating that the development of the bridging bidentate complex between the Zn atom and carboxylate involved C=O. In addition, some peaks altered after adsorption migrating upward or downward, where the intensity of other bands was seen to decrease. These studies demonstrated that chemisorption mechanisms such as hydrogen bonding, were responsible for the adsorption of LEV on ZnO nanosphere. Complexation, electrostatic contact, and the potential replacement of one of the hydroxyl groups in the ZnO nanosphere by a fluoride ion from the LEV are all possible.

Supported by the findings, which highlight the chemical adsorption, the complexes formed between the hydroxyl (–OH) groups on the LEV layer and the Zn(II) are likely responsible for the elimination of LEV. These substances frequently possess the (I) and (II) oxidation states and have a strong propensity to form covalent interactions with the soft head groups of adsorbent. The hard oxygen atoms of LEV do not appear to interact very favorably with the hard Zn(II) cations according to the findings that were obtained. However, prior studies indicate that the zinc ion has a unique coordination mechanism. Zn^{2+} behaves in its affinity towards O donors just like Cu^{2+}, which is relatively hard. Nevertheless, the availability of an appropriate main binding site is more significant. Consequently, Zn^{2+} exhibits an astounding attraction for hydroxyl groups. This crucial finding applies to nucleotides, nucleic acids, and other ligands that include hydroxyls. The ZnO effectiveness is implied by the adsorption ability, which is a variable [48,49].

3.4. Comparison studies

Table 6 compares the adsorption capability of the synthesized materials ZnO nanosphere with other adsorbents described in the literature for the adsorptive elimination of LEV. In comparison to most other adsorbents, the produced nanosphere showed a greater adsorption ability. However, the maximum adsorption capacity found in this study was less than those previously reported. Such results display the importance of ZnO adsorbent to remove the pollutant LEV from aqueous solution

3.5. Recycling and reusability of ZnO adsorbent

The re-usability properties of the ZnO nanosphere as an adsorbent for removing LEV from an aqueous medium were investigated. In comparison with the adsorption capacity in the first cycle with more cycles, the adsorption capacity somewhat declines. The differences between the original adsorption capacity and the obtained one in the fifth cycle were found to 15% meaning that the adsorbent kept more that 80% of the original adsorption amount. This occurrence showed how effectively ZnO nanospheres may be recycled and reused. The study analysed the ZnO material using XRD after three testing cycles and found that the crystallinity and structure were existence (Fig. 15). This study suggests that ZnO has a high degree of recyclability.

Table 6
Levofloxacin and ZnO nanospheres' abilities to bind to other adsorbents are compared

Adsorbent	q_m ($mg \cdot g^{-1}$)	References
Co-MCM-41	120	[50]
Fe/Mn-BC	181	[51]
Zeolite	35.5	[52]
CaO/MgO	107	[53]
MOFs, MIL-100 (Fe)	87.3	[54]
Fe_3O_4@SiO_2	6.85	[55]
ZnO	570.25	This work

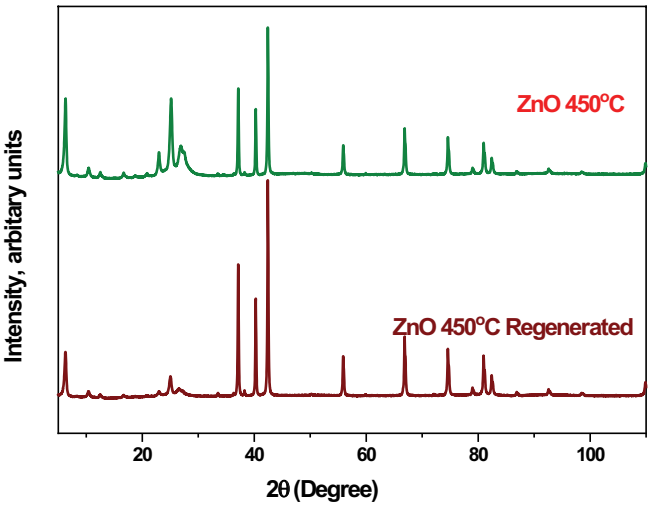

Fig. 15. X-ray diffraction spectra of ZnO 450°C and ZnO 450°C regenerated.

4. Conclusions

In this study, ZnO nanosphere via calcination of organo metallic chelate was successfully synthesized and further characterized with SEM, XRD, BET, and FT-IR. LEV was removed from the aqueous solution using the ZnO nanosphere. When everything is ideal at pH 6, the adsorption dose was 0.02 g with time 100 min. the adsorption kinetics is suitable for pseudo-second-order. Langmuir provided the greatest connect for the adsorption isotherm data and Dubinin–Radushkevich. Freundlich and Temkin provided additional support. Additionally, it was shown that LEV has a maximum adsorption capacity of 570.25 $mg \cdot g^{-1}$. The adsorbent was applied to real water samples and the percentage recoveries ranging from (85.17%–97.28%) were obtained. The created ZnO nanosphere was simple to remove and could be reused up to five times without losing its adsorption efficiency. The ZnO nanosphere's thermodynamic properties further demonstrated that the adsorption system was spontaneous and exothermic supporting the chemisorption process.

Acknowledgment

Princess Nourah bint Abdulrahman University Researchers Supporting Project number (PNURSP2022R92), Princess Nourah bint Abdulrahman University, Riyadh, Saudi Arabia.

Symbols

λ	—	Wavelength of X-ray, 1.54 Å
β	—	Compensated for instrumental expansion by the angular thickness of the peak at ZnO crystallite size determined at in height strength peak height at high intensity peak
β_{hkl}	—	Represents the full-width at half maximum (FWHM) of a radiant peak
β_s	—	Width due to the size–strain
β_D	—	Width due to the strain
D	—	Value of the crystallite size
ε	—	Value of the microstrain
q_e	—	Adsorbed amount of dye at equilibrium concentration, mmol·g^{-1}
q_{mL}	—	Maximum sorption capacity (corresponding to the saturation of the monolayer), mmol·g^{-1}
K_L	—	Langmuir binding constant which is related to the energy of sorption, L·mmol^{-1}
C_e	—	Equilibrium concentration of dyes in solution
K_F	—	Freundlich constants related to the sorption capacity, (mmol·g^{-1})(L·mmol^{-1})$^{1/n}$
n	—	Intensity
K_{DR}	—	Constant related to the sorption energy, J^2·mol^{-2}
q_{DR}	—	Theoretical saturation capacity, mmol·g^{-1}
ε	—	Polanyi potential, J^2·mol^{-2}
R	—	Gas constant, 8.314 J·mol^{-1}·K^{-1}
T	—	Temperature where the adsorption occurs
A_T	—	Temkin isotherm constant
b_T	—	Temkin constant in relation to heat of adsorption, J·mol^{-1}
q_t	—	Amount of dye adsorbed, mmol·g^{-1}
K_1	—	Rate constant for pseudo-first-order constant for the adsorption processes, min^{-1}
q_2	—	Maximum adsorption capacity for pseudo-second-order
K_2	—	Rate constant for pseudo-first-order constant for the adsorption processes, g·mg^{-1}·min^{-1}
α	—	Chemical adsorption rate, mg·g^{-1}·min^{-1}
β	—	Coefficient in relation with extension of covered surface
$\Delta G°$	—	Free Gibb's energy
$\Delta H°$	—	Enthalpy
$\Delta S°$	—	Entropy
K_c	—	Distribution coefficient
C_{eq}	—	Concentration at equilibrium, mg·L^{-1}

References

[1] A.K. Sarmah, M.T. Meyer, A.B.A. Boxall, A global perspective on the use, sales, exposure pathways, occurrence, fate and effects of veterinary antibiotics (VAs) in the environment, Chemosphere, 65 (2006) 725–759.
[2] E.M. Golet, I. Xifra, H. Siegrist, A.C. Alder, W. Giger, Environmental exposure assessment of fluoroquinolone antibacterial agents from sewage to soil, Environ. Sci. Technol., 37 (2003) 3243–3249.
[3] D. Fatta-Kassinos, S. Meric, A. Nikolaou, Pharmaceutical residues in environmental waters and wastewater: current state of knowledge and future research, Anal. Bioanal. Chem., 399 (2011) 251–275.
[4] C. Tong, X. Zhuo, Y. Guo, Occurrence and risk assessment of four typical fluoroquinolone antibiotics in raw and treated sewage and in receiving waters in Hangzhou, China, J. Agric. Food Chem., 59 (2011) 7303–7309.
[5] Y. Zhao, J. Geng, X. Wang, X. Gu, S. Gao, Adsorption of tetracycline onto goethite in the presence of metal cations and humic substances, J. Colloid Interface Sci., 361 (2011) 247–251.
[6] N. Genç, E.C. Dogan, Adsorption kinetics of the antibiotic ciprofloxacin on bentonite, activated carbon, zeolite, and pumice, Desal. Water Treat., 53 (2015) 785–793.
[7] A.A. El-Bindary, M.G. El-Desouky, M.A.M. El-Afify, Thermal and spectroscopic studies of some prepared metal complexes and investigation of their potential anticancer and antiviral drug activity against SARS-CoV-2 by molecular docking simulation, Biointerface Res. Appl. Chem., 12 (2021) 1053–1075.
[8] T.J. Al-Musawi, A.H. Mahvi, A.D. Khatibi, D. Balarak, Effective adsorption of ciprofloxacin antibiotic using powdered activated carbon magnetized by iron(III) oxide magnetic nanoparticles, J. Porous Mater., 28 (2021) 835–852.
[9] H.A. Kiwaan, F.Sh. Mohamed, N.A. El-Ghamaz, N.M. Beshry, A.A. El-Bindary, Experimental and electrical studies of Na-X zeolite for the adsorption of different dyes, J. Mol. Liq., 332 (2021) 115877, doi: 10.1016/j.molliq.2021.115877.
[10] D. Balarak, G. McKay, Utilization of MWCNTs/Al_2O_3 as adsorbent for ciprofloxacin removal: equilibrium, kinetics and thermodynamic studies, J. Environ. Sci. Health. Part A Toxic/Hazard. Subst. Environ. Eng., 56 (2021) 324–333.
[11] D. Balarak, N. Mengelizadeh, P. Rajiv, K. Chandrika, Photocatalytic degradation of amoxicillin from aqueous solutions by titanium dioxide nanoparticles loaded on graphene oxide, Environ. Sci. Pollut. Res., 28 (2021) 49743–49754.
[12] S. Su, W. Guo, C. Yi, Y. Leng, Z. Ma, Degradation of amoxicillin in aqueous solution using sulphate radicals under ultrasound irradiation, Ultrason. Sonochem., 19 (2012) 469–474.
[13] H. Pouretedal, N. Sadegh, Effective removal of amoxicillin, cephalexin, tetracycline and penicillin G from aqueous solutions using activated carbon nanoparticles prepared from vine wood, J. Water Process Eng., 1 (2014) 64–73.
[14] J.L. Acero, F.J. Benitez, F.J. Real, G. Roldan, Kinetics of aqueous chlorination of some pharmaceuticals and their elimination from water matrices, Water Res., 44 (2010) 4158–4170.
[15] D. Kapoor, Impact of pharmaceutical industries on environment, health and safety, J. Crit. Rev., 2 (2015) 25–30.
[16] H. Khazri, I. Ghorbel-Abid, R. Kalfat, M. Trabelsi-Ayadi, Removal of ibuprofen, naproxen and carbamazepine in aqueous solution onto natural clay: equilibrium, kinetics, and thermodynamic study, Appl. Water Sci., 7 (2017) 3031–3040.
[17] B. Kakavandi, A. Esrafili, A. Mohseni-Bandpi, A. Jonidi Jafari, R. Rezaei Kalantary, Magnetic Fe_3O_4@C nanoparticles as adsorbents for removal of amoxicillin from aqueous solution, Water Sci. Technol., 69 (2014) 147–155.
[18] N. Hassan, A. El-Sonbati, M. El-Desouky, Synthesis, characterization, molecular docking and DNA binding studies of Cu(II), Ni(II), Zn(II) and Mn(II) complexes, J. Mol. Liq., 242 (2017) 293–307.
[19] H. Liu, W. Liu, J. Zhang, C. Zhang, L. Ren, Y. Li, Removal of cephalexin from aqueous solutions by original and Cu(II)/Fe(III) impregnated activated carbons developed from lotus stalks: kinetics and equilibrium studies, J. Hazard. Mater., 185 (2011) 1528–1535.
[20] F. Wang, B. Yang, H. Wang, Q. Song, F. Tan, Y. Cao, Removal of ciprofloxacin from aqueous solution by a magnetic chitosan grafted graphene oxide composite, J. Mol. Liq., 222 (2016) 188–194.
[21] L. Benedini, D. Placente, J. Ruso, P. Messina, Adsorption/desorption study of antibiotic and anti-inflammatory drugs

onto bioactive hydroxyapatite nano-rods, Mater. Sci. Eng., C, 99 (2019) 180–190.
[22] W. Cai, M. Guo, X. Weng, W. Zhang, Z. Chen, Adsorption of doxorubicin hydrochloride on glutaric anhydride functionalized Fe_3O_4@SiO_2 magnetic nanoparticles, Mater. Sci. Eng., C, 98 (2019) 65–73.
[23] M.J. Ahmed, S.K. Theydan, Fluoroquinolones antibiotics adsorption onto microporous activated carbon from lignocellulosic biomass by microwave pyrolysis, J. Taiwan Inst. Chem. Eng., 45 (2014) 219–226.
[24] S. Carabineiro, T. Thavorn-Amornsri, M. Pereira, J. Figueiredo, Adsorption of ciprofloxacin on surface-modified carbon materials, Water Res., 45 (2011) 4583–4591.
[25] Y. Sun, Q. Yue, B. Gao, L. Huang, X. Xu, Q. Li, Comparative study on characterization and adsorption properties of activated carbons with H_3PO_4 and $H_4P_2O_7$ activation employing *Cyperus alternifolius* as precursor, Chem. Eng. J., 181 (2012) 790–797.
[26] Y. Yu, W. Wang, J. Shi, S. Zhu, Y. Yan, Enhanced levofloxacin removal from water using zirconium(IV) loaded corn bracts, Environ. Sci. Pollut. Res., 24 (2017) 10685–10694.
[27] P. Beigzadeh, F. Moeinpour, Fast and efficient removal of silver(I) from aqueous solutions using *Aloe vera* shell ash supported $Ni_{0.5}Zn_{0.5}Fe_2O_4$ magnetic nanoparticles, Trans. Nonferrous Met. Soc. China, 26 (2016) 2238–2246.
[28] J.Z. Pirhaji, F. Moeinpour, A.M. Dehabadi, S.A.Y. Ardakani, Synthesis and characterization of halloysite/graphene quantum dots magnetic nanocomposite as a new adsorbent for Pb(II) removal from water, J. Mol. Liq., 300 (2020) 112345, doi: 10.1016/j.molliq.2019.112345.
[29] S. Ghaderi, F. Moeinpour, F.S. Mohseni-Shahri, Removal of Zn(II) from aqueous solutions using $NiFe_2O_4$ coated sand as an efficient and low cost adsorbent: adsorption isotherm, kinetic and thermodynamic studies, Phys. Chem. Res., 6 (2018) 839–855.
[30] G. Peng, M. Zhang, S. Deng, D. Shan, Q. He, G. Yu, Adsorption and catalytic oxidation of pharmaceuticals by nitrogen-doped reduced graphene oxide/Fe_3O_4 nanocomposite, Chem. Eng. J., 341 (2018) 361–370.
[31] M.G. El-Desouky, M. Abd El-Wahab, A.A. El-Bindary., Interpretations and DFT calculations for polypropylene/cupper oxide nanosphere, Biointerface Res. Appl. Chem., 12 (2021) 1134–1147.
[32] M.A. El-Bindary, M.G. El-Desouky, A.A. El-Bindary, Metal–organic frameworks encapsulated with an anticancer compound as drug delivery system: synthesis, characterization, antioxidant, anticancer, antibacterial and molecular docking investigation, Appl. Organomet. Chem., 36 (2022) e6660, doi: 10.1002/aoc.6660.
[33] M.G. El-Desouky, M.A. Khalil, A.A. El-Bindary, M.A. ElBindary, Biological, biochemical and thermochemical techniques for biofuel production: an updated review, Biointerface Res. Appl. Chem., 12 (2022) 3034–3054.
[34] N. Hassan, A. Shahat, A. El-Didamony, M.G. El-Desouky, A.A. El-Bindary, Equilibrium, kinetic and thermodynamic studies of adsorption of cationic dyes from aqueous solution using ZIF-8, Moroccan J. Chem., 8 (2020) 624–635.
[35] H.A. Kiwaan, F.Sh. Mohamed, A.A. El-Bindary, N.A. El-Ghamaz, H.R. Abo-Yassin, M.A. El-Bindary, Synthesis, identification and application of metal organic framework for removal of industrial cationic dyes, J. Mol. Liq., 342 (2021) 117435, doi: 10.1016/j.molliq.2021.117435.
[36] M.G. El-Desouky, N. Hassan, A. Shahat, A. El-Didamony, A.A. El-Bindary, Synthesis and characterization of porous magnetite nanosphere iron oxide as a novel adsorbent of anionic dyes removal from aqueous solution, Biointerface Res. Appl. Chem., 11 (2021) 13377–13401.
[37] A.S. Al-Wasidi, I.I.S. AlZahrani, H.I. Thawibaraka, A.M. Naglah, M.G. El-Desouky, M.A. El-Bindary, Adsorption studies of carbon dioxide and anionic dye on green adsorbent, J. Mol. Struct., 1250 (2021) 131736, doi: 10.1016/j.molstruc.2021.131736.
[38] G.A.A. Al-Hazmi, M.A. El-Bindary, M.G. El-Desouky, A.A. El-Bindary, Efficient adsorptive removal of industrial dye from aqueous solution by synthesized zeolitic imidazolate framework-8 loaded date seed activated carbon and statistical physics modeling, Desal. Water Treat., 258 (2022) 85–103.
[39] K.O. Iwuozor, T.A. Abdullahi, L.A. Ogunfowora, E.C. Emenike, I.P. Oyekunle, F.A. Gbadamosi, J.O. Ighalo, Mitigation of levofloxacin from aqueous media by adsorption: a review, Sustainable Water Res. Manage., 7 (2021) 1–18.
[40] N. Hassan, A. Shahat, A. El-Didamony, M.G. El-Desouky, A.A. El-Bindary, Mesoporous iron oxide nano spheres for capturing organic dyes from water sources, J. Mol. Struct., 1217 (2020) 128361, doi: 10.1016/j.molstruc.2020.128361.
[41] T.A. Altalhi, M.M. Ibrahim, G.A.M. Mersal, M.H.H. Mahmoud, T.Kumeria, M.G. El-Desouky, A.A. El-Bindary, M.A. El-Bindary, Adsorption of doxorubicin hydrochloride onto thermally treated green adsorbent: equilibrium, kinetic and thermodynamic studies, J. Mol. Struct., 1263 (2022) 133160, doi: 10.1016/j.molstruc.2022.133160.
[42] C. Djilani, R. Zaghdoudi, F. Djazi, B. Bouchekima, A. Lallam, A. Modarressi, M. Rogalski, Adsorption of dyes on activated carbon prepared from apricot stones and commercial activated carbon, J. Taiwan Inst. Chem. Eng., 53 (2015) 112–121.
[43] S. Wong, N.A.N. Yac'cob, N. Ngadi, O. Hassan, I.M. Inuwa, From pollutant to solution of wastewater pollution: synthesis of activated carbon from textile sludge for dye adsorption, Chin. J. Chem. Eng., 26 (2018) 870–878.
[44] A.S. Al-Wasidi, I.I.S. AlZahrani, A.M. Naglah, M.G. El-Desouky, M.A. Khalil, A.A. El-Bindary, M.A. El-Bindary, Effective removal of methylene blue from aqueous solution using metal-organic framework; modelling analysis, statistical physics treatment and DFT calculations, ChemistrySelect, 6 (2021) 11431–11447.
[45] S. Lagergren, About the theory of so-called adsorption of soluble substances, J. Sven. Vetenskapsakad. Handingarl., 24 (1898) 1–39.
[46] G.A.A. AlHazmi, Kh.S. AbouMelha, M.G. El-Desouky, A.A. El-Bindary, Effective adsorption of doxorubicin hydrochloride on zirconium metal-organic framework: equilibrium, kinetic and thermodynamic studies, J. Mol. Struct., 1258 (2022) 132679, doi: 10.1016/j.molstruc.2022.132679.
[47] O.A. El-Gammal, F.Sh. Mohamed, G.N. Rezk, A.A. El-Bindary, Structural characterization and biological activity of a new metal complexes based of Schiff base, J. Mol. Liq., 330 (2021) 115522, doi: 10.1016/j.molliq.2021.115522.
[48] E. Zandi-Mehri, L. Taghavi, F. Moeinpour, I. Khosravi, S. Ghasemi, Designing of hydroxyl terminated triazine-based dendritic polymer/halloysite nanotube as an efficient nano-adsorbent for the rapid removal of Pb(II) from aqueous media, J. Mol. Liq., 360 (2022) 119407, doi: 10.1016/j.molliq.2022.119407.
[49] M.G. El-Desouky, A.A. El-Bindary, M.A. El-Bindary, Low-temperature adsorption study of carbon dioxide on porous magnetite nanospheres iron oxide, Biointerface Res. Appl. Chem., 12 (2022) 6252–6268.
[50] T.H. Tran, A.H. Le, T.H. Pham, D.T. Nguyen, S.W. Chang, W.J. Chung, D.D. Nguyen, Adsorption isotherms and kinetic modeling of methylene blue dye onto a carbonaceous hydrochar adsorbent derived from coffee husk waste, Sci. Total Environ., 725 (2020) 138325, doi: 10.1016/j.scitotenv.2020.138325.
[51] A.O. Dada, J. Ojediran, A.A. Okunola, F. Dada, A. Lawal, A. Olalekan, O. Dada, Modeling of biosorption of Pb(II) and Zn(II) ions onto PaMRH: Langmuir, Freundlich, Temkin, Dubinin–Raduskevich, Jovanovic, Flory–Huggins, Fowler–Guggenheim and Kiselev comparative isotherm studies, Int. J. Mech. Eng. Technol., 10 (2019) 1048–1058.
[52] H. Eyni, H. Tahermansouri, F. Kiani, M. Jahangiri, Kinetics, equilibrium and isotherms of Pb^{2+} adsorption from aqueous solutions on carbon nanotubes functionalized with 3-amino-5a,10a-dihydroxybenzo[b] indeno [2,ld]furan-10-one, New Carbon Mater., 34 (2019) 512–523.
[53] A. Dalalibera, P.B. Vilela, T. Vieira, V.A. Becegato, A.T. Paulino, Removal and selective separation of synthetic dyes from water using a polyacrylic acid-based hydrogel: characterization, isotherm, kinetic, and thermodynamic data, J. Environ. Chem. Eng., 8 (2020) 104465, doi: 10.1016/j.jece.2020.104465.

[54] Y. Liu, Y. Xiong, P. Xu, Y. Pang, C. Du, Enhancement of Pb(II) adsorption by boron doped ordered mesoporous carbon: isotherm and kinetics modeling, Sci. Total Environ., 708 (2020) 134918, doi: 10.1016/j.scitotenv.2019.134918.
[55] T. Sheela, Y.A. Nayaka, R. Viswanatha, S. Basavanna, T. Venkatesha, Kinetics and thermodynamics studies on the adsorption of Zn(II), Cd(II) and Hg(II) from aqueous solution using zinc oxide nanoparticles, Powder Technol., 217 (2012) 163–170.

Supporting information

S1. Chemicals

Chemicals were utilized exactly as they were supplied, without any further processing. They include zinc nitrate hexahydrate (99%, Tianjin Kemiou Chemical Reagent, China), dimethylformamide, anhydrous ethanol (99.7%, Sinopharm Chemical Reagent Co., Ltd., China) and levofloxacin standard solution were purchased Merck KGaA, 64271 Darmstadt, Germany.

S2. Characterization

Fourier-transform infrared spectra (KBr discs, 4,000–400 cm^{-1}) by Jasco-4100 Spectrophotometer. The structural differences of the as-prepared ZnO were investigated using the X-ray diffraction (XRD) method. The powder XRD patterns were captured using a Siemens D500 X-ray Diffractometer equipped with a Cu-Ka source of radiation. UV-Visible spectra from a Perkin Elmer AAnalyst 800 Spectrophotometer Model AAS with a 1.0 cm model system. The pH meter utilized was a WTW 720 Model Digital pH Meter. On ASAP 2020, the surface area was calculated to use the Brunauer–Emmett–Teller (BET) method, and the pore volume of the BET surfaces and the Barrett–Joyner–Halenda surface were calculated (Micrometrics, USA). Scanning electron microscopy (JEOL JSM-7600F, Japan) was used to examine the microstructure of ZnO. The specimen was then deposited onto a copper substrate after being sputter-coated with a homogenous gold layer. Energy-dispersive X-ray spectroscopy was used to analyze the elemental distribution of ZnO on a Leo1430VP Microscope with a 5 kV operating voltage.